

GCC and FBCC for linear tomosynthesis

Jérôme Lesaint, Simon Rit, Rolf Clackdoyle, Laurent Desbat

Abstract—Grangeat-based Consistency Conditions (GCC) and Fan-beam Consistency Conditions (FBCC) are two ways to describe consistency (or redundancy) between cone-beam projections. Here we consider cone-beam projections that are collected in the linear tomosynthesis geometry. We propose a theoretical comparison of these two sets of consistency conditions and illustrate the comparison with numerical simulations of a thorax Forbild phantom.

Index Terms—Cone-beam computed tomography (CBCT), data consistency conditions (DCCs), tomosynthesis.

I. INTRODUCTION

In Computed Tomography (CT), the 3D density map of a patient (or an object) is reconstructed from a set of 2D radiographs. Should the acquisition be realized in perfect conditions and neglecting physical side-effects (like scattering or beam-hardening), these radiographs (after their log-transform) follow the forward line-integral model. Unfortunately, these conditions are never fulfilled and systematic effects always degrade the projection data. One way to detect such effects is to quantify how inconsistent the data are, using the concept of data consistency conditions (DCC). DCC are equations that characterize the image of the forward operator. A large amount of research has been published on DCC. In parallel geometries, the well-known Helgason-Ludwig DCC [1], [2] provide necessary and sufficient conditions on the Radon transform. In divergent geometries, [3] and [4] also give necessary and sufficient conditions for a source moving along a linear trajectory (in 2D) or planar trajectory (in 3D) respectively. When a set of DCC is known to be complete (necessary *and* sufficient conditions), no additional information can be expected from another set of DCC. On the other hand, if two sets of DCC are known to be necessary but no information on the sufficiency is available, one may wonder which to use. Some works have introduced necessary-only conditions, like Grangeat-based DCC (GCC) [5], [6] and fan-beam DCC (FBCC) [3] extended to 3D projection data as suggested by [7]. As explained below, FBCC refers to what would be called zeroth-order conditions in [3].

Various applications of GCC and FBCC have been published. Geometric calibration in circular cone-beam CB [5] and in x-ray tomosynthesis [8] were described using GCC, and also jitter-

correction in x-ray CT [9]. For FBCC, a circular cone-beam micro CT application appeared recently [10].

In this work, we focus on GCC and FBCC and propose a theoretical comparison of these two sets of DCC. We carry this work in the specific context of tomosynthesis, with an X-ray source moving along a line. It is proved that the FBCC are stronger than the GCC, in the sense that if the FBCC are satisfied, then so are the GCC, but not conversely. We also show that if all the projections are complete (non-truncated) then the FBCC and GCC are equivalent. Furthermore the hypothesis of complete projections is essential; we show that under particular circumstances (with truncated projections), the FBCC are more restrictive, i.e., the FBCC can fail even when the GCC are satisfied. We finally prove that neither of these two sets of conditions are sufficient. The theory is detailed in Section II. Numerical aspects are presented in Section III and finally, Section IV contains discussion and conclusion.

II. THEORY

A. The forward X-ray model

We consider X-ray projection data g of an object function f , acquired along a 1D trajectory of the source parametrized by a scalar $\lambda \in \Lambda \subset \mathbb{R}$. The source position is denoted \vec{s}_λ . A projection g_λ associates to each unit vector $\vec{\alpha} \in \mathcal{S}^2$ the corresponding line integral:

$$g_\lambda(\vec{\alpha}) = \int_0^{+\infty} f(\vec{s}_\lambda + t\vec{\alpha}) dt. \quad (1)$$

B. The tomosynthesis geometry

In the following, we consider a tomosynthesis geometry, where an X-ray source moves along a line parallel to the plane of the detector. Let (O, x, y, z) be a 3D coordinate system. Without loss of generality, the detector, denoted \mathcal{D} , is assumed to lie in the $z = 0$ plane. It is equipped with 2D coordinates (O, u, v) where the detector origin O and the u - and v - axes coincide with the 3D origin and the x - and y - axes respectively. Note that the coordinates (u, v) are independent of the source position, as if the detector was large enough to capture every projection of the scan. (In the numerical simulations though, the detector was displaced horizontally.) The X-ray source moves along a line \mathcal{L} such that \vec{s}_λ has coordinates $(\lambda, 0, d)$ for $\lambda \in \Lambda$, where d is the source-to-detector distance and Λ is an interval. The object of interest is assumed to be entirely contained between \mathcal{D} and the plane parallel to \mathcal{D} and containing \mathcal{L} . See Figure 1.

C. The family of planes containing the source trajectory

We now focus on the family of planes which contain the source line. They will play an important role both in the

J. Lesaint, R. Clackdoyle and L. Desbat are with the TIMC-IMAG laboratory, CNRS UMR 5525 and Université Grenoble Alpes (e-mail : jerome.lesaint@univ-grenoble-alpes.fr).

S. Rit is with Univ. Lyon, INSA-Lyon, UCB Lyon 1, UJM-Saint Etienne, CNRS, Inserm, CREATIS UMR5220, U1206, Centre Léon Bérard, F-69373, LYON, France.

This work is partially supported by the Agence Nationale de la Recherche (France), Labex CAMI, number ANR-11-LABX-0004-01, Labex PRIMES, number ANR-11-LABX-0063 and project "DROITE", number ANR-12-BS01-0018.

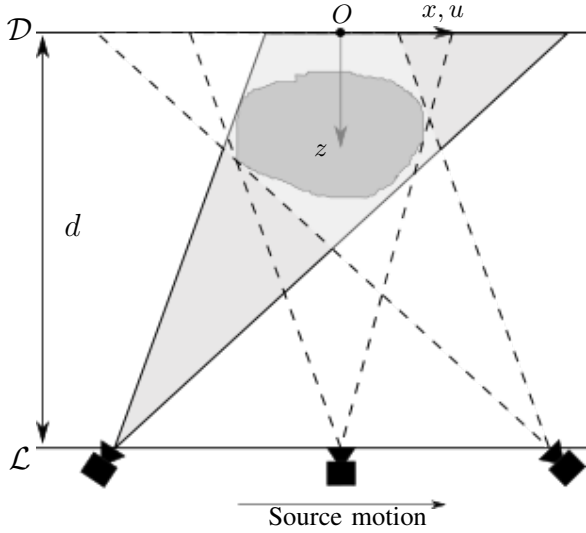


Fig. 1. Top-view of the tomosynthesis acquisition geometry. The X-ray source moves at constant distance d from the detector plane, along a horizontal line.

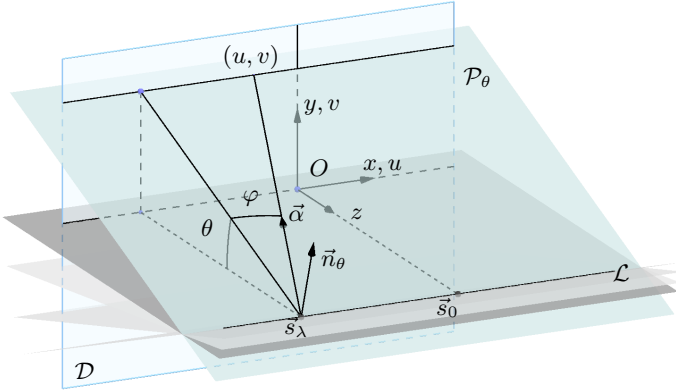


Fig. 2. The family of planes \mathcal{P}_θ . Each plane is defined by a normal vector \vec{n}_θ which makes an angle θ with the central plane. To each detector pixel (u, v) is associated a unit vector $\vec{\alpha}$ together with its spherical coordinates (θ, φ) .

Grangeat case and in the fan-beam case. For $\theta \in]-\frac{\pi}{2}; \frac{\pi}{2}[$, we let \mathcal{P}_θ denote the plane which contains the line \mathcal{L} and makes an angle θ with the central plane ($y = 0$). We let $\vec{n}_\theta = (0, \cos \theta, \sin \theta)$ denote the unit vector orthogonal to this plane. There is a one-to-one correspondence between the detector's horizontal rows (with offset v) and the planes \mathcal{P}_θ via the relation $d \tan \theta = v$. See Figure 2.

We assume that the detector is fixed so from detector coordinates (u, v) , the unit vector $\vec{\alpha}$ from Equation 1 is given by $\vec{\alpha} = ((u, v, 0) - \vec{s}_\lambda) / \|(u, v, 0) - \vec{s}_\lambda\| = (u - \lambda, v, -d) / \sqrt{(u - \lambda)^2 + v^2 + d^2}$. Furthermore $\vec{\alpha}$ can be expressed in spherical coordinates $\vec{\alpha}(\theta, \varphi) = (\sin \varphi, \cos \varphi \sin \theta, -\cos \varphi \cos \theta)$ where θ corresponds to the definition above, and φ is the latitude with respect to the polar axis x . (Note the unusual orientation of the spherical coordinates.) With a slight abuse of notation, we write

$g_\lambda(u, v) = g_\lambda(\vec{\alpha}(\theta, \varphi))$. We also use \tilde{g}_λ to denote the projection g_λ weighted by the cosine of the incidence angle of the ray. Given the coordinates of the source position $(\lambda, 0, d)$, we have:

$$\tilde{g}_\lambda(u, v) = g_\lambda(u, v) \frac{d}{\sqrt{(u - \lambda)^2 + v^2 + d^2}} \quad (2)$$

D. Grangeat-based consistency condition

Consistency conditions are equations derived from the forward model that ideal projection data must satisfy. Consistency conditions can be used to detect - and possibly correct for - inconsistencies introduced in the data by systematic effect such as mis-calibration, motion, scattering or beam-hardening.

Let $\mathcal{R}f(\mathcal{P}_\theta)$ denote the 3D Radon transform of f over the plane \mathcal{P}_θ . We recall the well-known result of Grangeat [11] (expressed with our notation):

$$\frac{1}{\cos^2 \theta} \frac{\partial}{\partial v} \int_{-\infty}^{+\infty} \tilde{g}_\lambda(u, v) du = \left. \frac{\partial}{\partial s} \mathcal{R}f(\mathcal{P}_\theta) \right|_{s=\vec{s}_\lambda \cdot \vec{n}_\theta} \quad (3)$$

where the derivative of $\mathcal{R}f$ is taken in the direction \vec{n}_θ . Again, v and θ are related through $v = d \tan \theta$.

For fixed \mathcal{P}_θ (equivalently, for fixed $v = d \tan \theta$), we note that $\vec{s}_\lambda \cdot \vec{n}_\theta = d \sin \theta$ is constant throughout the trajectory, so the right-hand-side of Equation 3 does not depend on the source position (it only depends on v , not on λ). We let $G(\lambda, v) = \frac{\partial}{\partial v} \int \tilde{g}_\lambda(u, v) du$, so the left-hand-side of Equation 3, $(1/\cos^2 \theta)G(\lambda, v)$, must be independent of λ . We thus obtain the following necessary DCC for this particular acquisition geometry:

The projection data $(g_\lambda)_{\lambda \in \Lambda}$ are consistent only if, for all v , $G(\lambda, v)$ is a constant function of λ .

This is what will be called in the sequel, the Grangeat-based Consistency Conditions, GCC for short.

Grangeat's result, Equation 3, is also the basis of Epipolar consistency conditions described in [6].

E. Fan-beam consistency conditions

Another way to quantify the redundancy/consistency of a set of projections is to fix the v coordinate and consider the corresponding plane \mathcal{P}_θ and the fan-beam projections therein. We then consider fan-beam consistency conditions (see [3] for a complete proof) extended to 3D cone-beam projections acquired in our particular tomosynthesis geometry: the set of projections $(g_\lambda)_{\lambda \in \Lambda}$ is consistent if and only if, for each $n = 0, 1, 2, \dots$ and each $\theta \in]-\frac{\pi}{2}; \frac{\pi}{2}[$, the function:

$$J_n(\lambda, \theta) = \int_{-\frac{\pi}{2}}^{\frac{\pi}{2}} \frac{g_\lambda(\alpha(\theta, \varphi))}{\cos \varphi} \tan^n \varphi d\varphi, \quad (4)$$

is a polynomial of order n in λ .

In particular, for $n = 0$, the quantity J_0 does not depend on the source position λ . It only depends on θ . And since there is a one-to-one correspondence between θ and v , we will write (with another small abuse of notation) $J_0(\lambda, v)$. These zeroth-order fan-beam consistency conditions will be referred to as FBCC. (When non-zero orders are being considered, we will state them explicitly.) These necessary conditions can be restated as:

The projection data $(g_\lambda)_{\lambda \in \Lambda}$ are consistent only if, for all v , $J_0(\lambda, v)$ is a constant function of λ .

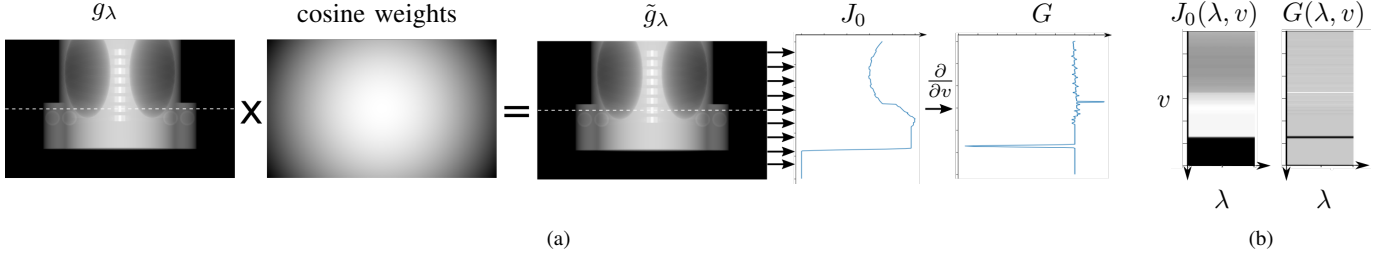


Fig. 3. a) Computation of both DCC for a single projection λ : projections g_λ are weighted with the cosine of the incidence angle. Integrals of \tilde{g}_λ over detector rows are computed: up to a fixed factor of d , this is $J_0(\lambda, v)$. For each λ , $J_0(\lambda, v)$ is differentiated with respect to v to get $G(\lambda, v)$. The dotted line indicates the detector row used in Figures 5 and 6. b) The functions $J_0(\lambda, v)$ and $G(\lambda, v)$ plotted as gray-value images. Note that the gray scales are different in the two.

F. Relationships between FBCC and GCC

We can now prove the theoretical contribution of this abstract:

Proposition 1 (FBCC \Rightarrow GCC). *If the projection data satisfy FBCC, then they necessarily satisfy GCC.*

Before proving this statement, a few comments are in order. First, the proposition means that (order-0) FBCC carry at least as much information as GCC. Second, under some specific circumstances, we will prove that this assertion is strict, in the sense that we can design a projection example which satisfies GCC but breaks FBCC. Finally, neither GCC nor FBCC are sufficient consistency conditions because the zeroth-order fan-beam conditions alone are insufficient; it was shown in [3] that all orders $n = 0, 1, 2, \dots$ are necessary and sufficient.

Proof of Proposition 1: We start with FBCC (Equation 4) and change the spherical variables (θ, φ) to the (u, v) detector coordinates with $v = d \tan \theta$ and $u = \sqrt{v^2 + d^2} \tan \varphi$. After elementary computations, we get:

$$J_0(\lambda, v) = \frac{1}{d} \int_{-\infty}^{+\infty} \tilde{g}(u, v) du. \quad (5)$$

The FBCC state that for each v , J_0 is a constant function of λ . Therefore, $J_0(\lambda, v)$ is independent of λ . Now, it is clear from the definition of G that:

$$G(\lambda, v) = d \frac{\partial}{\partial v} J_0(\lambda, v), \quad (6)$$

which proves that G is also independent of λ . Therefore, for each v , $G(\lambda, v)$ is a constant function of λ , so the GCC are satisfied and the proof is complete. ■

If the converse of this statement holds then the two sets of DCC would be equivalent.

Proposition 2 (FBCC \Leftrightarrow GCC). *The FBCC and GCC are equivalent in the ideal case of untruncated projections.*

Proof of Proposition 2: In light of Proposition 1, we only need to prove that if the GCC are satisfied, then the FBCC are satisfied. From Equation 6, we obtain:

$$J_0(\lambda, v) = \frac{1}{d} \int G(\lambda, v) dv + \kappa_\lambda, \quad (7)$$

where κ_λ depends on λ but not on v . The GCC are assumed to be satisfied, so $G(\lambda, v)$ is independent of λ , and therefore the integral term in Equation 7 is also independent of λ . So for

each λ , $J_0(\lambda, v)$ is the same function of v except for the additive constant κ_λ (which varies with λ). Now, since the projections are assumed to not be truncated, there exist some v^* (which corresponds to an actual row of the physical detector) such that:

$$\forall \lambda \in \Lambda, \forall v \geq v^* \quad g_\lambda(u, v) = 0. \quad (8)$$

In particular, $g_\lambda(u, v^*) = 0$ for all λ , and therefore $J_0(\lambda, v^*) = 0$ for all λ . For each λ , the functions (of v) $J_0(\lambda, v)$ all agree for $v = v^*$, and therefore the additive offsets κ_λ must be the same, so $\kappa_\lambda = \kappa$ is a constant (independent of λ). Therefore $J_0(\lambda, v)$ is independent of λ and the FBCC are satisfied. ■

We now show that the hypothesis of untruncated projections cannot be relaxed in Proposition 2.

Proposition 3. *FBCC and GCC are not equivalent; a counter-example.*

Proof of Proposition 3: Let us modify one single projection g_{λ_0} as follows:

$$\gamma_{\lambda_0}(u, v) = g_{\lambda_0}(u, v) + \frac{\sqrt{(u - \lambda_0)^2 + v^2 + d^2}}{Ld}. \quad (9)$$

Note that the modified projection is non-zero everywhere, so it would be considered a truncated projection and would not satisfy the hypotheses of Proposition 2. The added term is the inverse of the cosine of the incidence angle, weighted by the inverse of the width of the detector (L). It is easily seen that this modification adds a constant term to $J_0(\lambda_0, v)$ for all v , hence breaks the FBCC without affecting the GCC. ■

Note that this modification of the projection is equivalent (up to a constant) to filtering the X-ray beam with a flat filter of constant thickness, placed perpendicularly to the z -axis.

III. NUMERICAL SIMULATIONS

We simulated 40 projections of a thorax Forbild phantom (see Figure 3a for a sample projection). The acquisition geometry was described in Section II-B. The source-to-detector distance was fixed at 600 mm. The source positions were $(\lambda, 0, 600)$ where λ varies evenly from -200 mm to $+190$ mm. The detector size was 500×300 pixels, with pixel size 0.3 mm^2 . In our reference projections, the phantom center of mass was placed at $(0, 12, 300)$ (centered in x , at mid-distance between the source and the detector plane and with a vertical offset of 12 mm). All simulations were carried out with the Reconstruction ToolKit

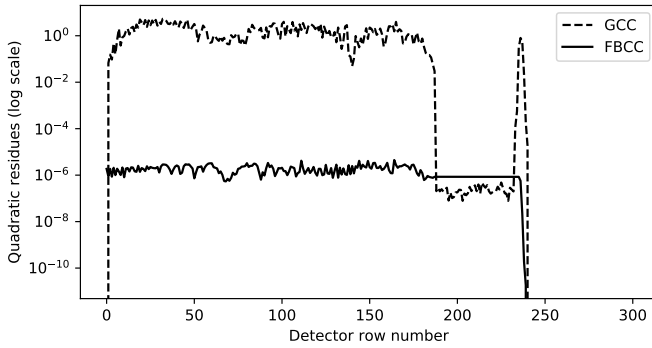


Fig. 4. Quadratic residues of the linear regression of the functions $G(\lambda, v)$ and $J_0(\lambda, v)$ as a function of v . On the last 60 detector rows, the signal is 0, so are G and J_0 . The residues are not represented on this log-scale figure.

(RTK, [12]). The implementation of FBCC in this set up only requires a sum over the rows of the projections. The derivative in the v -direction involved in GCC is implemented with a central finite difference. Note that the two DCC involve computing line integrals in the u -direction of the projection images. Hence, projections must not be truncated in that direction.

A. Are G and J_0 constant ?

Saying that the projection data satisfy GCC or FBCC amounts to saying that for each v (i.e. each detector row), the 1D functions $G(\cdot, v)$ and $J_0(\cdot, v)$ are constant functions of λ . For each projection, we computed $G(\lambda, v)$ and $J_0(\lambda, v)$ for all v according to Equations 3 and 4 respectively (see Figure 3a) and concatenated those 1D signals to get 300 (number of detector rows) supposedly constant signals (see Figure 3b). To quantify how constant those signals were, we computed the slope of their linear regression. In both cases (FBCC and GCC), the mean over all planes and the standard deviation were numerically zero, as stated by the theory. To further investigate the respective behavior of each consistency measure, for each v we computed the sum of squared difference between the signals $G(\cdot, v)$ and $J_0(\cdot, v)$ and their regression line. These residues are presented in Figure 4.

Both the GCC and FBCC results are theoretical in the sense that the functions G and J_0 cannot be exactly constant in λ practically since they required numerical approximation of integrals. The errors in this approximation are amplified by the differentiation step in the computation of G . This amplification of the discretization errors is the probable explanation for why the residues for G are 10^6 times greater than J_0 .

B. Illustration of inconsistency

We examined the effect on the GCC and FBCC of a small rigid motion of the object. After 20 projections, the phantom was displaced vertically and 15 projections were collected in the displaced position. The phantom was then returned to the original position for the last 5 projections. We repeated the study with 3 different magnitudes of displacement: 2.5 mm, 1.0 mm, and 0.2 mm. We restricted the study to one plane

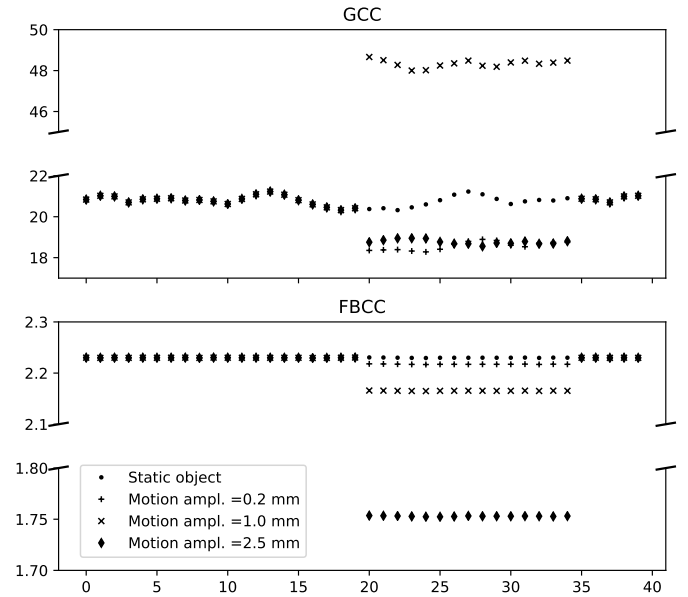


Fig. 5. Sensitivity of each DCC to a vertical motion of the object. The object is displaced between projections 20 and 35.

(row index 150) when calculating the consistency conditions. Figure 5 shows that $G(\lambda, v)$ and $J_0(\lambda, v)$ were both constant (to within small numerical errors) for the consistent collections of projections, but that the constant changed when the object was displaced to a new position. As the displacement became larger, the change in FBCC increased, as was expected. On the other hand, the GCC over-reacted to the 1.0 mm displacement, due to particular features of the phantom.

C. FBCC and GCC are not sufficient conditions

In order to illustrate the fact that both GCC and FBCC are not sufficient conditions, we simulated 40 projections of the same phantom which was displaced horizontally (in the x -direction) at projection 20 and left in the displaced position for the remaining projections. The first and last 20 projections alone were consistent, but not the full 40 projections. Since both GCC and FBCC involve computations of integrals along horizontal detector rows, it is intuitive that they will fail in detecting inconsistencies resulting from motion in the horizontal direction. In Figure 6, we show that FBCC and GCC erroneously indicate consistent data (both are constant as expected), while FBCC-1 detects inconsistency (severe discontinuity in $J_1(\lambda)$, the theoretical order-1 polynomial) when the object was displaced. This study was conducted in the plane corresponding to the row index 192. (This plane is such that J_0 and G have the same order of magnitude, which facilitates convenient plotting on a single figure.)

IV. DISCUSSION AND CONCLUSION

In this abstract we proved that FBCC carry at least as much information as GCC. In the non-truncated case, FBCC and GCC are equivalent and in the truncated case, we designed projection

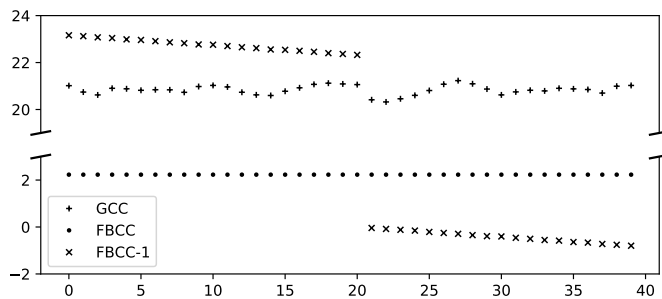


Fig. 6. From projection index 20, the object was moved horizontally by 5 mm. While GCC and FBCC fail to detect the inconsistency induced by the motion, FBCC-1 does.

data which satisfy GCC but not FBCC. We illustrated that both the GCC and FBCC are not sufficient conditions for this tomosynthesis geometry. In practice, neither of the DCC are perfectly satisfied, due to numerical errors in the quadrature methods involved in FBCC and GCC. Based on our simulation studies, the FBCC seem to be more robust to GCC in the presence of numerical errors.

REFERENCES

- [1] S. Helgason, *The Radon transform*, ser. Progress in mathematics. Boston, Basel, Berlin: Birkhäuser, 1999. [Online]. Available: <http://opac.inria.fr/record=b1095821>
- [2] D. Ludwig, "The radon transform on euclidean space," *Communications on Pure and Applied Mathematics*, vol. 19, no. 1, pp. 49–81, 1966. [Online]. Available: <http://dx.doi.org/10.1002/cpa.3160190105>
- [3] R. Clackdoyle, "Necessary and Sufficient Consistency Conditions for Fanbeam Projections Along a Line," *IEEE Transactions on Nuclear Science*, vol. 60, no. 3, pp. 1560–1569, 2013.
- [4] R. Clackdoyle and L. Desbat, "Full data consistency conditions for cone-beam projections with sources on a plane," *Physics in Medicine and Biology*, vol. 58, no. 23, p. 8437, 2013. [Online]. Available: <http://stacks.iop.org/0031-9155/58/i=23/a=8437>
- [5] C. Debbeler, N. Maass, M. Elter, F. Dennerlein, and T. M. Buzug, "A New CT Rawdata Redundancy Measure applied to Automated Misalignment Correction," in *The 12th International Meeting on Fully Three-Dimensional Image Reconstruction in Radiology and Nuclear Medicine*, Lake Tahoe, USA, 2013, pp. 264–267. [Online]. Available: <http://www.fully3d.org/2013/Fully3D2013Proceedings.pdf>
- [6] A. Aichert, M. Berger, J. Wang, N. Maass, A. Doerfler, J. Hornegger, and A. K. Maier, "Epipolar Consistency in Transmission Imaging," *IEEE Transactions on Medical Imaging*, vol. 34, no. 11, pp. 2205–2219, nov 2015.
- [7] M. S. Levine, E. Y. Sidky, and X. Pan, "Consistency Conditions for Cone-Beam CT Data Acquired with a Straight-Line Source Trajectory," *Tsinghua science and technology*, vol. 15, no. 1, pp. 56–61, 2010. [Online]. Available: <http://www.ncbi.nlm.nih.gov/pmc/articles/PMC2886312/>
- [8] T. Grulich, W. Holub, U. Hassler, A. Aichert, and A. Maier, "Geometric Adjustment of X-ray Tomosynthesis," in *Proceedings of the 13th International Meeting on Fully Three-Dimensional Image Reconstruction in Radiology and Nuclear Medicine.*, 2015, pp. 468–471.
- [9] N. Maass, F. Dennerlein, A. Aichert, and A. Maier, "Geometrical Jitter correction in computed tomography," in *Proceedings of the third international conference on image formation in x-ray computed tomography*, Salt Lake City, USA, 2014, pp. 338–342.
- [10] J. Lesaint, S. Rit, R. Clackdoyle, and L. Desbat, "Calibration for Circular Cone-Beam CT Based on Consistency Conditions," *IEEE Transactions on Radiation and Plasma Medical Sciences*, vol. 1, no. 6, pp. 517–526, 2017. [Online]. Available: <http://ieeexplore.ieee.org/document/7999272/>
- [11] P. Grangeat, "Mathematical framework of cone beam 3D reconstruction via the first derivative of the radon transform," in *Mathematical Methods in Tomography*, ser. Lecture Notes in Mathematics, G. Herman, A. Louis, and F. Natterer, Eds. Springer Berlin Heidelberg, 1991, vol. 1497, pp. 66–97. [Online]. Available: <http://dx.doi.org/10.1007/BFb0084509>

- [12] S. Rit, M. V. Oliva, S. Brousmiche, R. Labarbe, D. Sarrut, and G. C. Sharp, "The Reconstruction Toolkit (RTK), an open-source cone-beam CT reconstruction toolkit based on the Insight Toolkit (ITK)," *Journal of Physics: Conference Series*, vol. 489, no. 1, p. 12079, 2014. [Online]. Available: <http://stacks.iop.org/1742-6596/489/i=1/a=012079>